Jurnal Tribologi 46 (2025) 58-79

MYTRIBOS Malaysian Tribology Society

Jurnal Tribologi

Website : jurnaltribologi.mytribos.org e-issn: 2289-7232

Impact of slip and surface roughness on journal bearing performance: A CFD and FSI approach

Muchammad Muchammad [1*], Mohammad Tauviqirrahman [1], Dimas A. Alamsyah [1], Imam Syafa'at [2]

[1] Mechanical Engineering, University of Diponegoro, INDONESIA.
[2] Mechanical Engineering, University of Wahid Hasyim, INDONESIA.
[*]Corresponding author: m_mad5373@yahoo.com

KEYWORDS

CFD
Fluid-Solid Interaction (FSI)
Partial rough surface
Slip-wall
Multistep journal bearing

ABSTRACT

Journal bearings are widely utilized in industries, such as automotive, power generation, and marine applications. This study examines the performance of the lubrication system in both plain and multistep journal bearings for tribological properties, including hydrodynamic pressure, load-carrying capacity, and friction force. The bearings are subjected to various surface roughness conditions, together with slip-wall formations. Computational fluid dynamics is employed to simulate this analysis under cavitation conditions. This study applied fluid-structure interaction to investigate the deformation in the bearings. The modeling results demonstrate that surface roughness substantially affects the maximum hydrodynamic pressure in the convergent region. The slip-wall surface increases hydrodynamic pressure on the journal bearing. A greater reduction in maximum hydrodynamic pressure was noted on Ra 6.3 μm compared to Ra 0.2 μm and Ra 0.8 μm, indicating a decline in lubricating efficacy relative to surface roughness. The tribological parameters generally show that the multistep journal bearing is superior to the plain journal bearing. The study did not consider thermal or transient effects. Experimental research is the next step in confirming the simulation results.

Received 7 October 2024; received in revised form 17 March 2025; accepted 1 April 2025.
To cite this article: Muchammad et al. (2025). Impact of slip and surface roughness on journal bearing performance: A CFD and FSI approach. Jurnal Tribologi 46, pp.58-79.

1.0 INTRODUCTION

A bearing is a component commonly utilized in machining systems. Journal bearings, a subtype of hydrodynamic bearings, are frequently used in rotors subjected to heavy loads (Zapomel & Ferfecki, 2022; Sayed & El-Sayed, 2022). Hydrodynamic bearings utilize a fluid to create hydrodynamic pressure, thereby separate the rotating shaft from the bearing housing and supporting the shaft's load (Oliveira et al., 2022). Journal bearings operate on the theory of utilizing a lubricating fluid as a separator to prevent contact between the rotating shaft and the inner surface of the bearing. Numerous methods exist to enhance the performance of the lubricating system in journal bearings, including surface texturing. This texture is considered a fluid reservoir in lack of lubricating fluid (Lu & Khonsari, 2007).

Bompos et al. (2016) simplified complex geometric structures into a multistep journal bearing. This type is more straightforward due to its reduced number of existing indentations, although it possesses a greater surface area, hence enhancing the storage capacity of the lubricating fluid. The lubricating fluid used in the lubrication of journal bearings will experience cavitation when situated in the diverging zone (Tauviqirrahman et al. 2016). The cavitation phenomena can result from variations in pressure values in the convergent and divergent regions of journal bearings. This process leads the lubricant to transition into steam (Dhande and Pande, 2016). Cavitation in textured bearings must be prevented, as it can diminish load-carrying ability, as indicated in several studies (Gropper et al. (2016); Muchammad et al. (2020); Syafaat et al. (2024)). A significant finding from cavitation investigations indicates that modeling must account for cavitation conditions.

Analysis of journal bearings working under high circumstances, it is essential to determine the elastohydrodynamic lubrication conditions (Chen et al., 2019). Benasciutti et al. (2012) performed a static analysis of elastohydrodynamic journal bearings. The elastic deformation of the journal bearing part resulted in a more uniform pressure distribution. The deformation will affect the boundary condition of the lubrication part of the fluid domain (Shenoy, 2010). This makes analytical modeling is essential to account for the interaction between the fluid domain and the solid domain. Previous research concentrated on hydrodynamic lubrication analysis (Dhande & Pande, 2017); however, under conditions of elevated pressure and temperature, journal bearings undergo elastic deformation (Kumar et al., 2020), which impacts the clearance distance of the bearing. To achieve consistent bearing performance, it is essential to conduct an elastohydrodynamic (EHD) lubrication analysis of the journal bearing (Chen et al., 2019; Hili et al., 2010; Prabhakaran et al., 2007).

Liu et al. (2010) performed a study utilizing the Computational Fluid Dynamics - Fluid-Structure Interaction (CFD-FSI) approach for the examination of EHD lubrication. This research determined that elastic deformation in EHD lubrication substantially influenced the locus position. Additionally, Chalkiopoulos et al. (2020) performed a thermoelastohydrodynamic (TEHD) lubrication investigation on journal bearings. TEHD lubrication is a journal bearing lubrication method that considers both mechanical and thermal loads. The analysis identified an increase in elastic deformation occurring in the bearing. Consequently, mechanical-thermal stress was incorporated in this research. In addition to surface roughness, the condition of slippery surfaces can also influence the lubrication performance of journal bearings. In a study by Cui et al. (2019), the impact of introducing slip-wall areas on plain journal bearings was examined. Their research found that applying a slip-wall area in the convergent region of plain journal bearings enhanced performance by up to 4.5%.

In real-world conditions, not only does deformation impact the lubrication performance of journal bearings, but the condition of the bearing surface also plays a significant role. Sander et al. (2016) identified differences between the surface of a new journal bearing and one with a rough surface, specifically a reduction in maximum contact pressure. A study by Tauviqirrahman et al. (2019), Muchammad et al. (2021), and Muchammad et al. (2024) investigated the effect of surface roughness on journal bearing modeling using the CFD-FSI method, taking into account the influence of deformation on lubrication. The findings indicated that the lubrication performance of journal bearings decreases when deformation is considered, and the rougher the bearing surface, the lower its lubrication performance.

The examination of several literatures indicates that enhancing hydrodynamic pressure and load-bearing capability necessitates the development of a journal bearing with a textured surface. Furthermore, the implementation of a slip-wall might augment the generated pressure. Conversely, research regarding the impact of surface roughness combined with slip engineering remains notably scarce. The application of Computational Fluid Dynamics (CFD) incorporating the deformation of the bearing structure through Fluid-Structure Interaction (FSI) is frequently employed to model the lubrication system. This study intends to examine the effects of surface roughness using two distinct bearing designs: plain bearings and multistep bearings, utilizing computational fluid dynamics (CFD). This study presents a textured surface design implemented as a multistep journal bearing featuring several grooves on its surface.

2.0 METHODOLOGY

2.1 Governing Equations

In fluid flow, the Navier–Stokes equation consists of a set of equations that describe the motion of a fluid. This equation indicates that the change in momentum of fluid particles is determined solely by the internal viscous forces and the external pressure forces acting upon the fluid. Consequently, the Navier–Stokes equation represents the force equilibrium in Newtonian fluids undergoing viscous flow, adhering to the principle of momentum conservation. The mass conservation equation is presented as follows (Chen et al., 2019).

$$\frac{\partial \rho_f}{\partial t} + \nabla.(\rho_f \vec{v}) = 0 \tag{1}$$

Where ∇ in equation (1) represents the vector operator, ρ_f represents the density of the lubricating fluid, $\vec{V}$ represents the velocity vector of the lubricating fluid, and trefers to the time utilized for the calculation of the lubricating fluid.

The equation of conservation of momentum can be determined in equation (2) (Chen et al., 2019):

$$\frac{\partial}{\partial t}(\rho_f \vec{v}) + \nabla.(\rho_f \vec{v}\vec{v}) = -\nabla.P + \nabla.\left(\vec{\vec{\tau}}\right) + \rho_f \vec{g} + \vec{F} \tag{2}$$

Where P represents the static pressure, $\vec{g}$ and $\vec{F}$ each is the gravitational force and the external force. While $\bar{\bar{\tau}}$ in equation (3) is the tension tensor that can be defined using this following equation (Chen et al., 2019).

$$\bar{\bar{\tau}} = \mu_f \left[\left(\nabla \vec{v} + \nabla \vec{v}^T \right) - \frac{2}{3} \nabla . \vec{v} I \right] \tag{3}$$

Where μ_f and I respectively are the dynamic viscosity of the fluid and the tensor unit.

2.2 Slip Modelling

The boundary condition on a surface can be transformed into a slippery surface by altering the property condition and the constraints of its roughness (Tauviqirrahman et al., 2021). In the slip surface condition, the flow velocity at the surface is unaffected by deceleration from shear stress. In the slip model, the limiting condition of the slip wall occurs when the fluid's shear stress surpasses the critical shear stress limit in equation (4).

$$\text{If } \tau < \tau_{cr}, u_s = 0 \text{ and If } \tau \geq \tau_{cr}, u_s = (\tau - \tau_{cr}) \frac{b}{\mu} \tag{4}$$

Where u_s represents slip velocity, b is the length of the slip viewing area, and μ is the viscosity of the lubricant. For a comprehensive understanding of slip theory and its applications, readers are encouraged to review the works of Muchammad et al. (2020) and Syafaat et al. (2024).

2.3 Cavitation Modelling

In the lubrication system of journal bearings, cavitation may occur due to a drop in pressure below atmospheric levels, reducing the fluid's capacity to dissolve air and resulting in the formation of air bubbles within the fluid layer. Additionally, cavitation can arise when the lubricant pressure falls below the saturated vapor pressure, causing the lubricant to change phases into vapor. Under actual conditions, cavitation significantly impacts the performance of a journal bearing's lubrication system. The collapse of air bubbles generates high-pressure shock waves, potentially damaging the performance and surface of the journal bearing.

According to Dhande & Pande (2017), when modeling cavitation in journal bearings with an inlet at the top and an outlet on the side, the Zwart-Gerber-Belamri model demonstrates superior modeling capabilities. This model assumes that all bubbles within the system are of the same size and aims to calculate the total mass transfer between phases per unit based on bubble density.

$$\text{If } P < P_v, \; R_e = F_{evap} \frac{3\alpha_{nuc}(1-\alpha_v)\rho_v}{R_B} \sqrt{\frac{2(P_v - P)}{3\rho_l}} \tag{5}$$

$$\text{If } P \geq P_v, \; R_c = F_{cond} \frac{3\alpha\rho_v}{R_B} \sqrt{\frac{2(P_v - P)}{3\rho_l}} \tag{6}$$

In the equation (5) and (6), F_{evap} = evaporation coefficient = 50, F_{Cond} = condensation coefficient = 0.01, R_B = bubble radius = 10^{-6} m, α_{nuc} = nucleation site volume fraction = 5×10^{-4}, ρ_l = liquid density, P_v = vapor pressure.

2.4 Surface Roughness

Surface roughness refers to a common texture observed on a material's surface. It is typically measured by the deviation of the surface's normal vector from its ideal shape. A greater deviation suggests a higher surface roughness value. The surface roughness is often quantified using the roughness average (Ra).

In ANSYS software, surface roughness can be modeled as a uniform roughness, represented by the roughness height (Ks) (ANSYS, 2016). The conversion of this parameter to the arithmetic mean surface roughness (Ra) can be achieved using the algorithm provided by Czaban (2014) and (Adams et al., 2012) resulting in the equation (7).

$$\mathrm{K_s} = 5.863\ \mathrm{R_a} \tag{7}$$

The surface roughness of a material is influenced by the grinding process, which reduces particle size from a coarse shape to smaller, finer sizes.

2.5 Fluid-Structure Interaction (FSI)

Lubrication in journal bearings involves the interplay between pressure and the deformation that may occur in the bearing materials. Therefore, understanding the interaction between the solid and fluid components is crucial. This interaction within the lubrication system of journal bearings presents a fluid-structure interaction (FSI) problem. Such a condition establishes a relationship between the forces exerted by the fluid domain and the resulting deformation in the solid domain, and vice versa. These interactions can lead to changes in the existing boundary conditions, which can be described by the equations (8-10) (Yanzhen et al., 2016).

$$d_f = d_s \tag{8}$$

$$\mathrm{n} \cdot \tau_\mathrm{f} = \mathrm{n} \cdot \tau_\mathrm{s} \tag{9}$$

$$T_f = T_s \tag{10}$$

where d_f and d_s represent as displacement in the fluid domain and solid domain. τ_f and τ_s represent as the stress in the fluid domain and solid domain. T_f and T_s represent as the temperature in the fluid domain and the solid domain.

The governing equations of the fluid and solid domains are integrated into a matrix system, as illustrated in the equation (11) (Yanzhen et al., 2016).

$$\begin{bmatrix} A_{ff} & A_{fs} \\ A_{sf} & A_{ss} \end{bmatrix} \begin{bmatrix} \Delta X_f^k \\ \Delta X_s^k \end{bmatrix} = \begin{bmatrix} F_f \\ F_s \end{bmatrix} \tag{11}$$

where A_{ff}, A_{ss}, A_{fs}, dan A_{sf} represent as a system matrix of fluid, solid, and coping effects, sequentially. ΔX_f^k and ΔX_s^k are a solution from Fluid and Solid Domain. F_f and F_s are the external force of the fluid and solid domain. All equations pertaining to fluid-structure interaction are resolved using Ansys software. This study selects the CFD-FSI method due to its capacity to forecast structural deformation by integrating phenomena in both fluid and solid domains. These advantages have been referenced in various prior publications in the Introduction section.

2.6 Model and Boundary Conditions

This lesson uses the geometry of a plain journal bearing, with dimensions based on a simulation by Dhande & Pande (2017). This work included an investigation of the impact of multistep surface application on the performance of the journal bearing lubrication system. The multistep texture geometry is derived from the journal bearing geometry presented by Bompos and Nikolakopoulos (2016). The geometric schema is illustrated in Figures 1 and 2. The geometric parameters and material qualities utilized in this investigation are presented in Table 1 and Table 2. This study is constrained by several factors: the fluid employed is characterized as Newtonian and incompressible, the simulation is conducted under steady-state and isothermal conditions, and the flow modeling is based on k-ε turbulent flow dynamics.

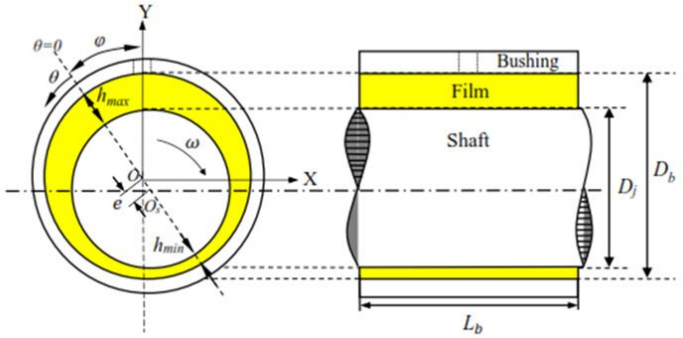

(a)

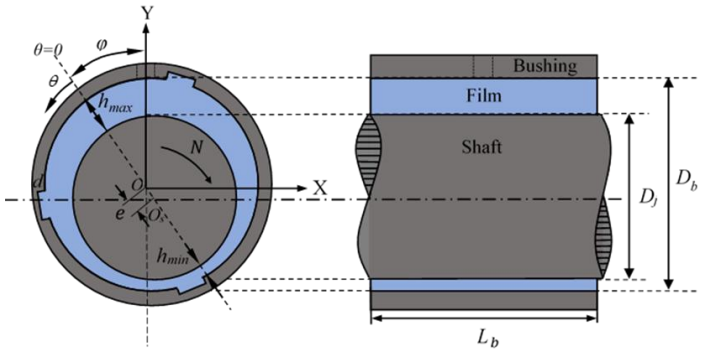

(b)

Figure 1: Geometry and coordinate system (a) plain bearing; (b) multistep journal bearing.

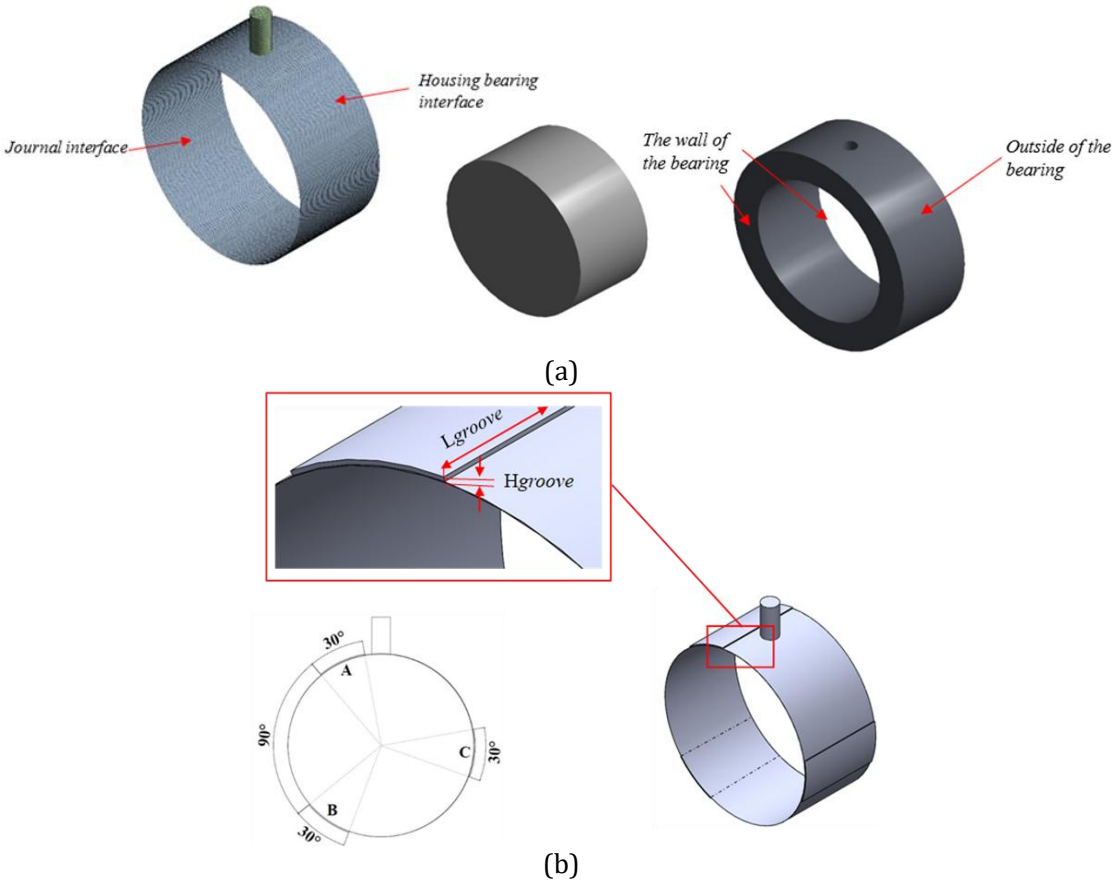

Figure 2: Physical model (a) plain bearing; (b) multistep journal bearing.

Table 1: Parameters used in numerical analysis.

Parameters		**Parameters**	
Plain Journal Bearing		Groove Length	25 mm
Clearance, c	0.05 mm	Groove height	0,3 mm
Diameter, d	50 mm	**Lubricant parameters**	
Length, L	25 mm	Oil density, ρ_f	850 kg/m^3
Eccentricity ratio, ε	0.8	Oil liquid viscosity, μ_o	0,0125 Pa.s
Attitude angle, φ	55°	Oil vapour density, ρ_V	10,95 kg/m^3
Multistep Journal Bearing		Oil vapour viscosity, μ_V	2×10^{-5} Pa.s
Step arc angle	30°	Vaporization pressure, P_v	29,185 Pa
Angle between steps	90°		

Table 2: Structure parameters used in numerical analysis.

Structure parameters		**Structure parameters**	
Journal: Steel		**Housing: Aluminium**	
Elastic modulus, E_S	210 GPa	Elastic modulus, E_A	68.3 GPa
Density, ρ_S	7,850 kg/m^3	Density, ρ_A	2,700 kg/m^3
Poison ratio, υ_S	0.3	Poison ratio, υ_A	0.33
Yield Strength	2,5x10^8 Pa	Yield Strength	2,8x10^8 Pa

2.7 Solution Method

In this simulation, before configuring the boundary condition values (see Table 3), the meshing stage is performed. The purpose of meshing is to achieve simulation results that closely approximate accuracy. In fluid-structure interaction simulations, meshing is applied to both the fluid and solid domains.

In this study, meshing is conducted for each journal bearing geometry. The total number of elements used in the plain journal bearing simulation is 153,302 for the fluid domain and 187,030 for the solid domain. For the multistep journal bearing, the solid domain consists of 186,030 elements, while the fluid domain contains 156,302 elements.

Table 3: Boundary conditions.

Boundary	**Condition**
Inlet	Pressure inlet (0 Pa)
Outlet	Pressure outlet (1 atm)
	Stationary wall
The journal interface	Moving wall (3,000 rpm)
The outside of the housing	Cylindrical support
The wall of the housing	Displacement

In the surface roughness simulation, the roughness values applied are categorized as Fine, Medium, and Rough. Within the ANSYS simulation, the roughness level (*Ra*) is converted to the roughness height (*Ks*) value. The specific roughness values are presented in Table 4. The selection of various roughness numbers in this study is based on the machining process previously examined in the paper by Muchammad et al. (2024).

Table 4: Roughness value parameters.

R_a (µm)	**K_s (m)**	**Level**
0,2	1,173 x 10^{-6}	Fine
0,8	4,69 x 10^{-6}	Medium
6,3	3,694 x 10^{-5}	Rough

3.0 RESULTS AND DISCUSSION

3.1 Validation Study

The validation case is based on a simulation by Dhande and Pande (2017). The validation was performed by comparing the results of the current simulation with those obtained by Dhande and Pande. The comparison focuses on the maximum hydrodynamic pressure value and the deformation value of the bearing.

A sensitivity assessment of the mesh was conducted before data collection. The results for mesh independence are illustrated in Figure 3. The meshing of about 153,000 elements demonstrates an insignificant variation (0.284%) in the resultant pressure of 5.63 MPa, despite the increase in the number of elements.

In the simulation conducted by Dhande and Pande (2017) (see Figure 4 and 5), the maximum pressure contour obtained was 5.528 MPa, whereas the current simulation yielded a maximum pressure of 5.625 MPa. This results in a 1.72% difference in the Pmax value between the two simulations. Additionally, there is a variation in the deformation of the journal bearing bushing. In the simulation by Dhande and Pande, the deformation was 0.4831 μm, while the current simulation shows a deformation of 0.4957 μm. This corresponds to a deviation of 2.39% in the bushing deformation.

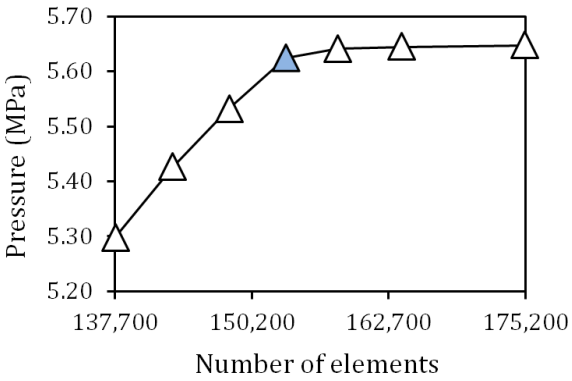

Figure 3: Mesh independence study in journal bearing modeling. The quantity of elements, 153,000, was chosen for further analysis due to the absence of a significant rise in the generated pressure despite a substantial increase in the number of elements.

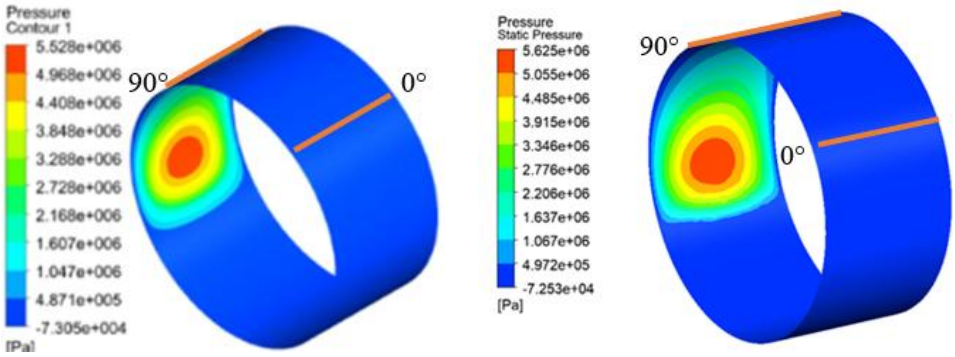

(a) (b)

Figure 4: Comparison of Pressure Distribution Contours of Journal Bearing (a) Dhande and Pande Simulation (2017) with FSI and (b) Present Study with FSI.

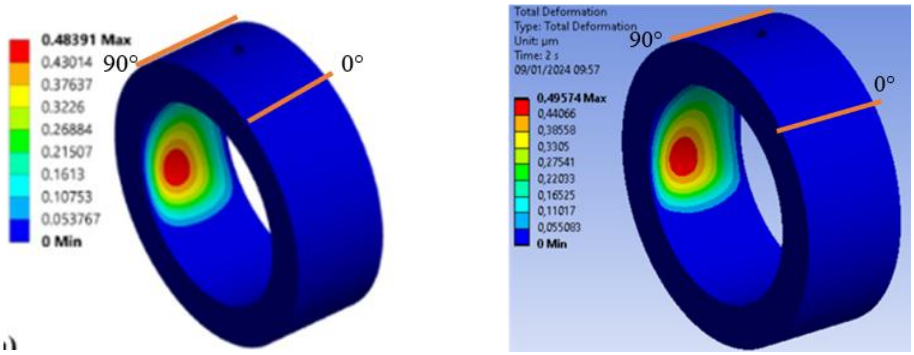

(a) (b)

Figure 5: Comparison of Journal Bearing Deformation Contours (a) Dhande and Pande Simulation (2017) with FSI and (b) Present Study with FSI.

3.2 Effect of Slip Surface on Journal Bearing

In this simulation, a performance analysis of the journal bearing is conducted on the slip surface. Under slip surface conditions, the flow velocity in contact with the journal bearing surface does not decrease due to shear stress. The surface tension in the slip-wall area is set to zero. Introducing slip surface conditions alters the lubrication performance of the journal bearing, with one of the affected parameters being the generated hydrodynamic pressure. The distribution contours of hydrodynamic pressure are shown in Figure 6(a). In plain journal bearings, the hydrodynamic pressure increases from 5.625 MPa to 7.128 MPa. In contrast, for multistep bearings, the pressure rises from 6.090 MPa to 7.544 MPa.

The effect of the change in hydrodynamic pressure can be observed in Figure 8(a). For the plain journal bearing, the Load-Carrying Capacity (LCC) on the slip-wall surface increased from 1909 N to 2095 N. This rise is attributed to the increase in hydrodynamic pressure during bearing operation, as shown in the graph in Figure 6. However, for the multistep journal bearing, the LCC on the slip-wall surface decreased from 2050 N to 1818 N. This reduction in LCC may be due to a

narrowing of the area under the pressure curve. Although the hydrodynamic pressure increases, the overall pressure area is reduced, as depicted in the graph in Figure 7.

Figure 6 illustrates that the peak pressure is observed at an angle of 180° in the model devoid of slip treatment. The maximum pressure in the wall-slip simulation occurs several degrees later and generates larger hydrodynamic pressure than the model without slip. This demonstrates that slip engineering can augment pressure and alter the peak pressure position. In contrast to Tønder's (2001) research, which shown that positioning the inlet near the leading edge can enhance hydrodynamic pressure; the findings of this study are inconsistent with his conclusions. This results from the impact of the eccentricity ratio in this study, which leads to a constriction of the lubrication zone, thereby generating hydrodynamic pressure at a position of about 180°.

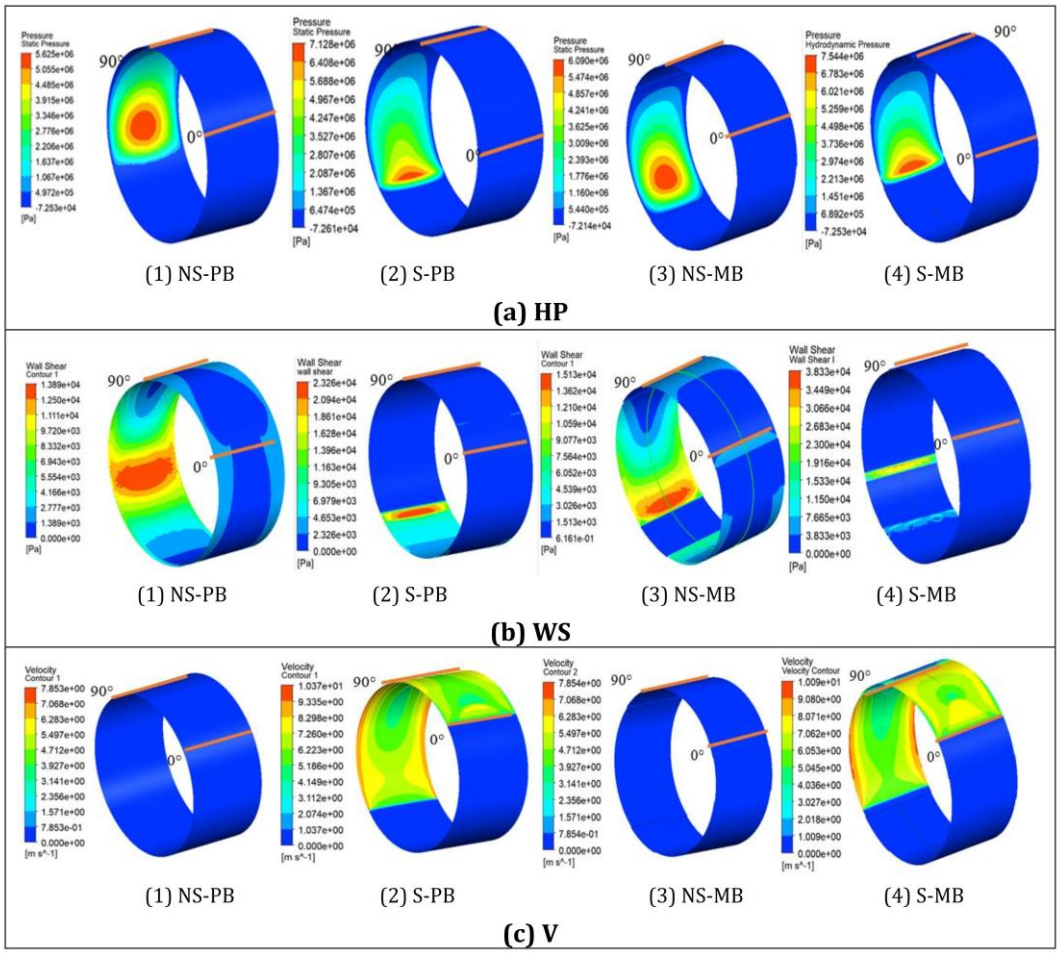

Figure 6: Comparison of no slip plain bearing [NS-PB] (1), plain bearing with slip condition [S-PB] (2), no slip multistep bearing [NS-MB] (3), multistep bearing with slip condition [S-MB] (4). (a) Hydrodynamic pressure - HP; (b) Wall Shear - WS; (c) Velocity - V.

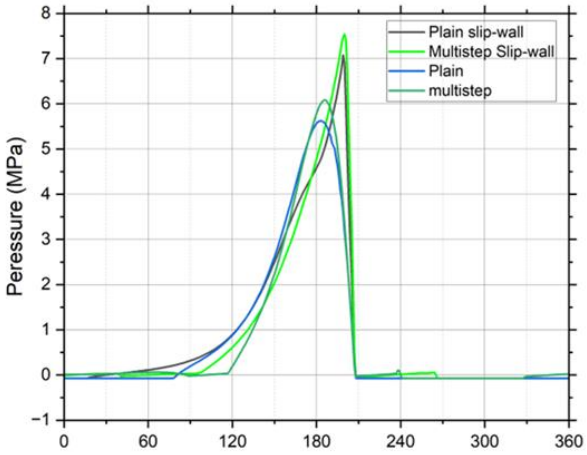

Figure 7: Hydrodynamic pressure distribution graph on a journal bearing.

The effect of the change in hydrodynamic pressure can be observed in Figure 8(a). For the plain journal bearing, the Load Carrying Capacity (LCC) on the slip-wall surface increased from 1909 N to 2095 N. This rise is attributed to the increase in hydrodynamic pressure during bearing operation, as shown in the graph in Figure 6. However, for the multistep journal bearing, the LCC on the slip-wall surface decreased from 2050 N to 1818 N. This reduction in LCC may be due to a narrowing of the area under the pressure curve. Although the hydrodynamic pressure increases, the overall pressure area is reduced, as depicted in the graph in Figure 7.

According to Figure 6(b), applying slip conditions reduces the area where shear stress occurs. By eliminating shear stress, the velocity of the fluid flow in contact with the surface is not slowed down by the wall's shear pressure, as shown in Figure 6(c). Consequently, the reduction in the shear stress area leads to a decrease in the friction force within the bearing, which is illustrated in Figure 8(b). The present study observed the inclusion of slip can enhance LCC in the context of plain bearings, as illustrated in Figure 8(a). In the model devoid of slip (smooth model), the multistep bearing configuration results in significant LCC. The grooves on the multistep bearing's surface facilitate ample lubricant supply, resulting in increased pressure and subsequently elevated LCC. The application of additional lubricant reduces the frictional force (Figure 8(b)). In industrial applications, hydrophobic properties, particularly the capacity to generate a slip effect, can be attained using chemical or physical methods. This can be accomplished by creating surface roughness akin to that of a lotus leaf (Ivanović, et al., 2018). A chemical procedure is utilized using coating technology. It is essential to consider the production challenges to comprehend this slip state (Syafaat et al., 2024).

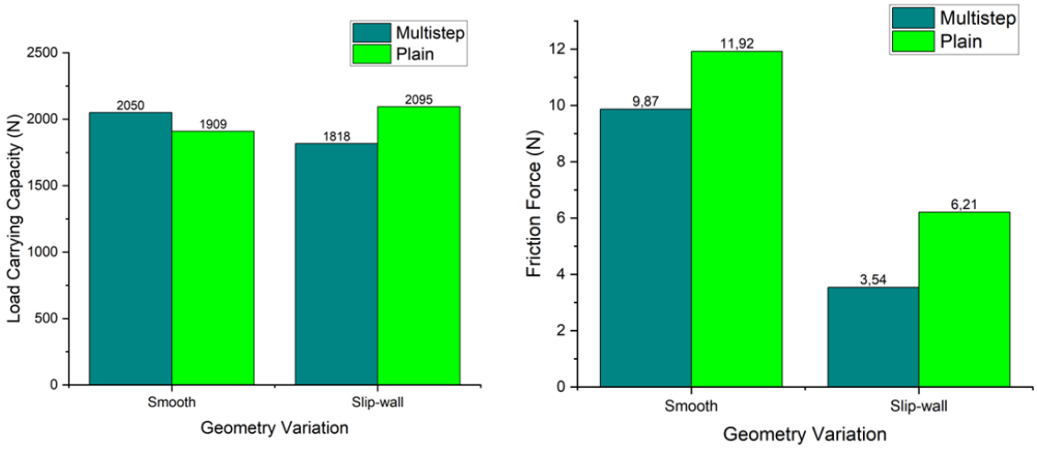

(a) (b)

Figure 8: Effect of providing slip surfaces on plain and multistep journal bearings. (a) Load carrying capacity; (b) Friction Force.

Figure 9(a) illustrates the effect of deformation in plain journal bearings, showing that applying a slip surface increases the hydrodynamic pressure, which in turn results in greater deformation on the bushing surface. The deformation in plain bearings rises from 0.495 μm to 0.508 μm. A similar phenomenon is observed in multistep journal bearings, as shown in Figure 9(b), where the deformation increases to 0.558 μm due to the application of the slip surface.

3.3 Effect of Surface Roughness on Plain and Multistep Journal Bearings

One of the key processes in manufacturing bearings is grinding, which influences the surface roughness quality. This roughness is characterized by the roughness height (*Ks*). This simulation compares the lubrication performance in plain journal bearings and multistep journal bearings with varying roughness, *Ra*: 0.2, 0.8, and 6.3 μm.

As shown in Figure 10(a), in plain journal bearings, there is a decline in hydrodynamic pressure as surface roughness increases. The maximum hydrodynamic pressure on a plain bearing with *Ra* 0.2 is 5.263 MPa, which decreases to 3.20 MPa at *Ra* 6.3. Figure 10(b) indicates that multistep journal bearings exhibit a similar trend; however, at the rough level, there is an increase in pressure, but the area of maximum pressure is reduced. The pressure distribution of hydrodynamic pressure is depicted in Figure 11. Figures 10(c) and 10(d) display the distribution of wall shear stress along the lubricating surface of the journal bearing. This shear stress influences the frictional force experienced by the bearing during operation.

According to Figure 11, the LCC, which represents the integral calculation of pressure across the fluid layer's surface, decreases as the roughness increases. In plain journal bearings, as shown in Figures 10(a), 11(a), and 12(a), the LCC at different roughness levels are: 1,747 N for *Ra* 0.2, 1,381 N for *Ra* 0.8, and 1,138 N for *Ra* 6.3 μm.

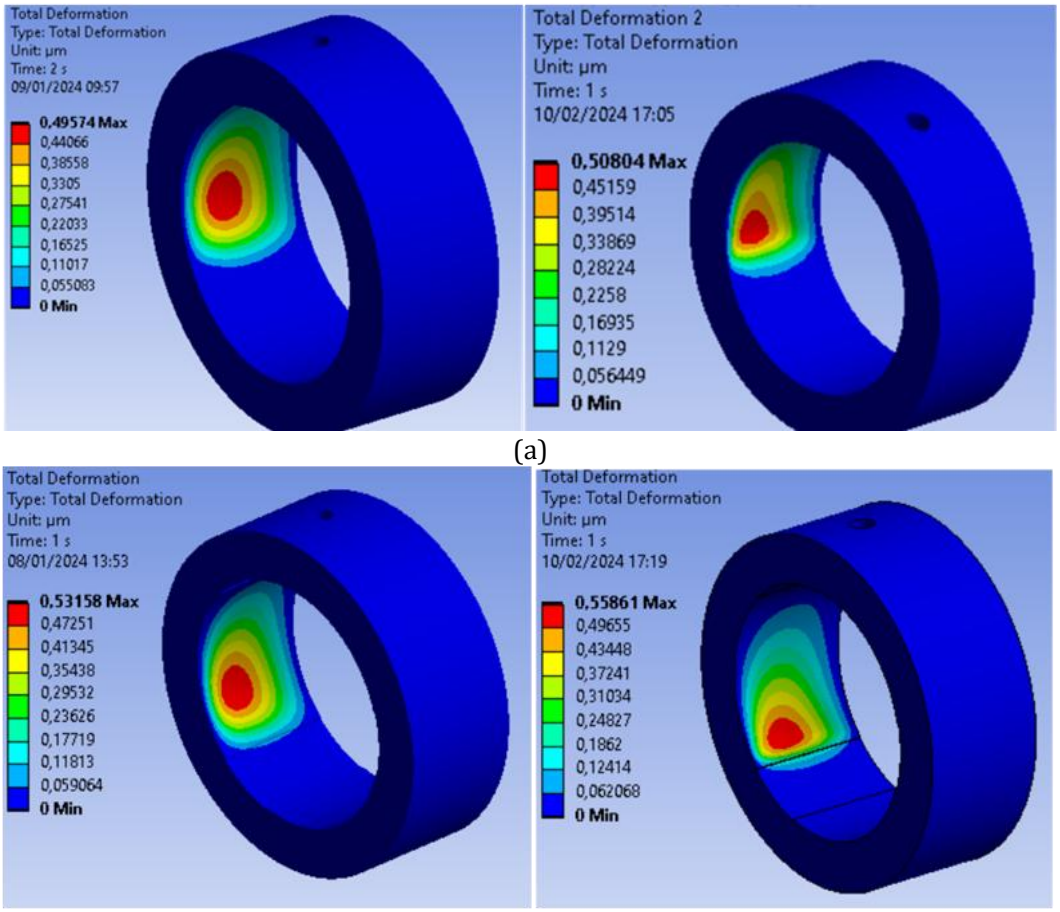

Figure 9: Bushing deformation on; (a) Plain bearing; (b) Multistep bearing.

Although Figure 10(b) indicates an increase in hydrodynamic pressure at rough roughness levels, the graph in Figure 11(b) reveals a narrowing of the area under the rough roughness pressure curve. This leads to a reduction in LCC, as seen in Figure 12(a), with LCC values for multistep journal bearings at 1,945 N for *Ra* 0.2, 1,815 N for *Ra* 0.8, and 1,749 N for *Ra* 6.3 µm. This indicates that the LCC diminishes with increasing roughness. High roughness levels can disrupt the flow of the lubricant, leading to an uneven lubricating film. Additionally, increased roughness may result in the uneven distribution of lubricants, creating zones of low pressure and consequently reducing the maximum hydrodynamic pressure.

Figures 10(c) and 10(d) show that the distribution contours of wall shear stress are spread along the surface. In multistep journal bearings, the distribution of wall shear is different from that in plain journal bearings, where it is more evenly distributed. The highest wall shear occurs in the convergence area, specifically the step area following the attitude angle or pressure formation zone. The contours reveal that, in areas with rough surfaces, the wall shear is concentrated in a narrow region between the rough surface and the adjacent smooth surface.

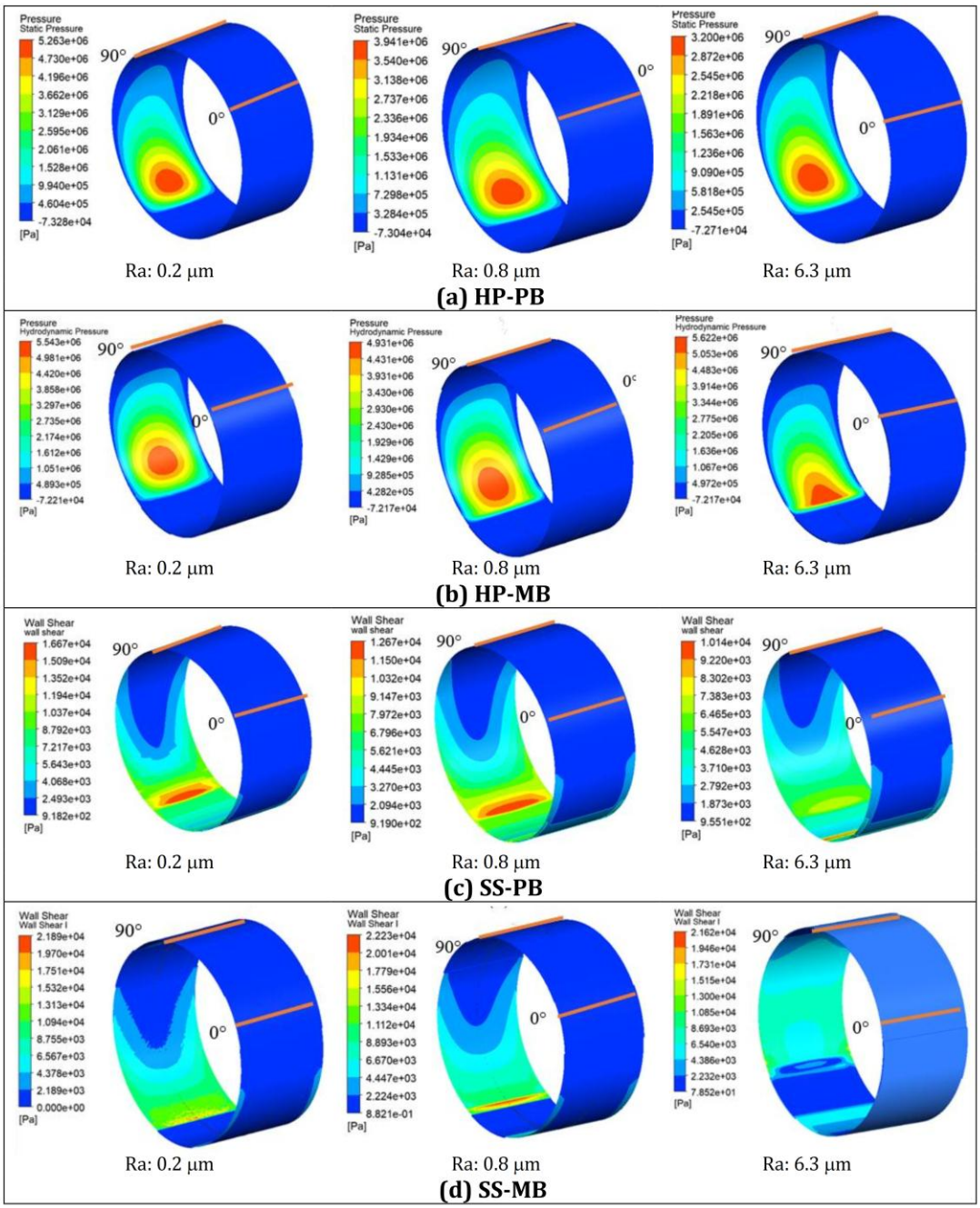

Figure 10: Comparison of *Ra* 0.2 µm, *Ra* 0.8 µm, *Ra* 6.3 µm. (a) HP-PB: Hydrodynamic pressure of plain bearing; (b) HP-MB: Multistep journal bearing hydrodynamic pressure; (c) SS-PB: Shear stress on plain bearings; and (d) SS-MB: Shear stress on Multistep journal bearings.

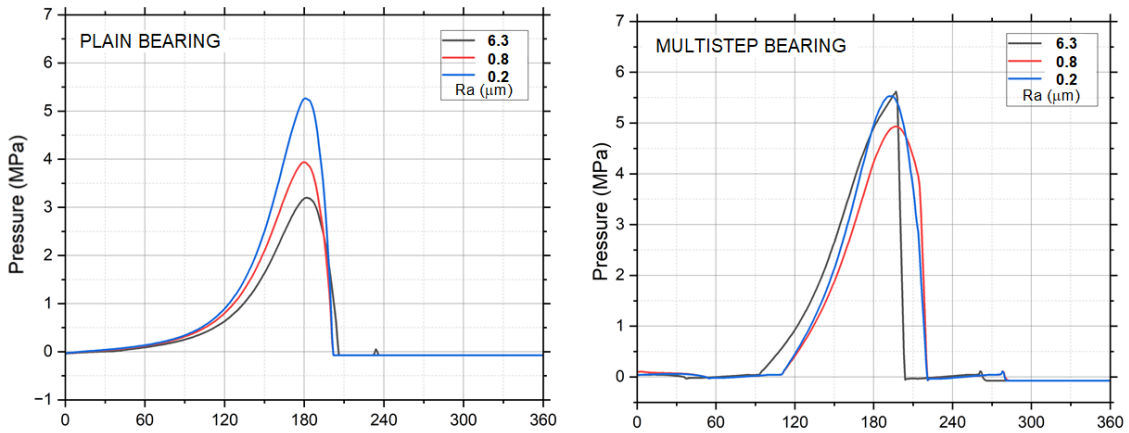

Figure 11: Hydrodynamic pressure distribution graph, (a) Plain bearing; (b) Multistep journal bearing of the varied surface roughness.

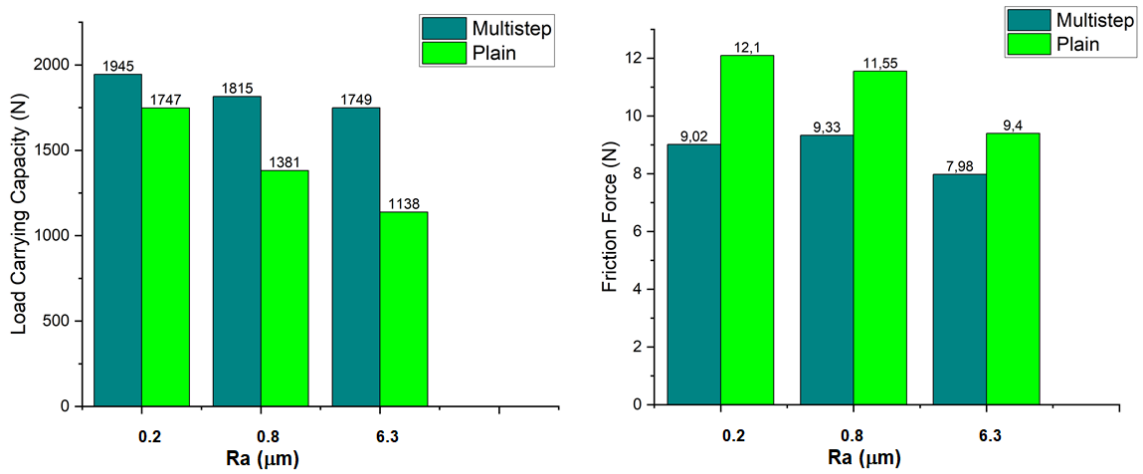

Figure 12: Effect of providing slip surfaces on plain and multistep journal bearings. (a) Load carrying capacity; (b) Friction Force.

As shown in Figure 12(b), the friction force values at different levels of surface roughness for plain journal bearings are 12.1 N for *Ra* 0.2, 11.55 N for *Ra* 0.8, and 9.4 N for *Ra* 6.3 μm. In contrast, for multistep journal bearings, the friction force values are 9.02 N for *Ra* 0.2, 9.33 N for *Ra* 0.8, and 7.98 N for *Ra* 6.3 μm.

This study demonstrated that in both bearing types, a rougher surface correlates with a reduced LCC. Since LCC depends on the amount of pressure and surface area, rough surfaces (asperities) diminish the area that requires lubrication. The reduction in this region results in a corresponding drop in the LCC. The research indicated the multistep textured bearing design exhibits a greater LCC than the plain untextured type, as illustrated in Figure 12 (a). The rationale for this is that the multistep design offers a greater microreservoir of lubrication within the

groove compared to the plain bearing type. This is the reason the LCC exceeds that of the plain bearing. As the lubricant supply increases, the frictional force diminishes (Figure 12 (b)). The findings of the current study align with the research conducted by Muchammad et al. (2024).

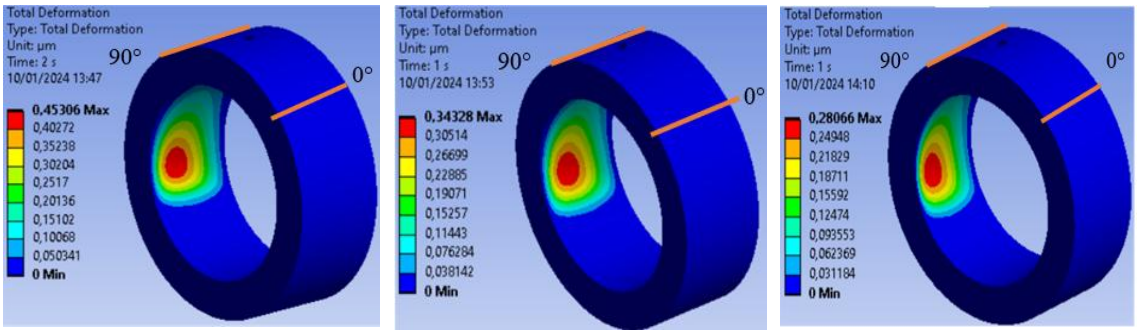

(a)

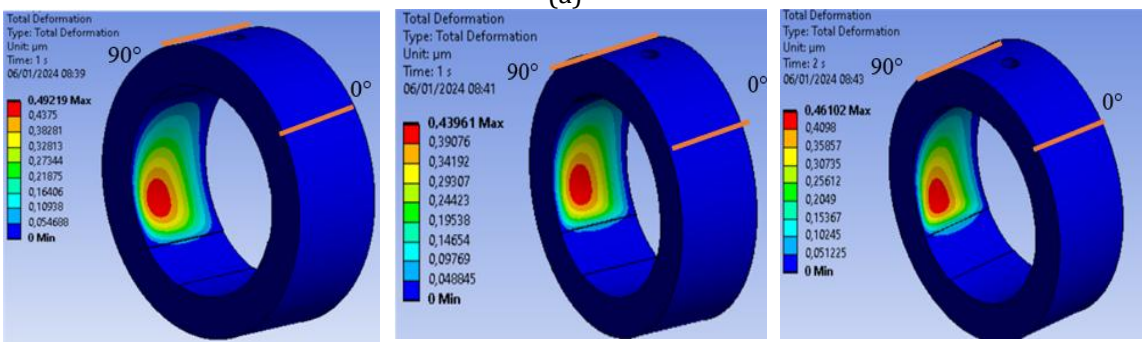

(b)

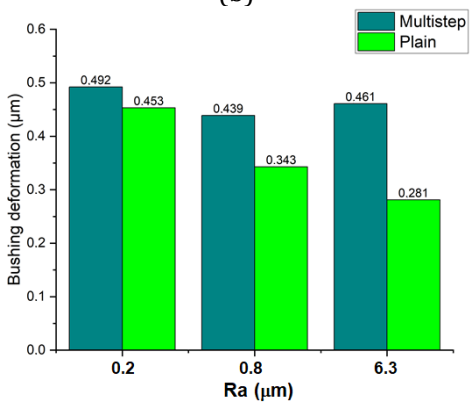

(c)

Figure 13: Comparison of varied of surface roughness in two types of journal bearings, (a) deformation in plain bearings; (b) deformation in multistep journal bearing; (c) deformation graph.

Figure 13 illustrates the impact of these roughness variations on the deformation of journal bearing bushings. The deformation is a result of the mechanical load applied by the lubrication system as the bearing rotates. As shown in Figure 11(a), the decrease in hydrodynamic pressure

for plain bearings leads to a reduction in deformation, which is evident in Figures 13(a) and 13(c), where the deformation values are provided. In contrast, for multistep journal bearings, changes in the deformation contour are observed in Figure 13(b). The increase in hydrodynamic pressure on rough surfaces, as seen in Figure 11(b), results in higher deformation for multistep journal bearings. The application of a slip surface to the journal bearing influences its lubrication performance, particularly the resulting hydrodynamic pressure. When considering surface roughness, an increase in roughness leads to a decrease in hydrodynamic pressure on the journal bearing.

3.4 Cavitation On Plain and Multistep Journal Bearings

This article does not explicitly address cavitation; rather, this section will provide a quick explanation of the topic. Besides being influenced by pressure, the cavitation phenomenon must also be examined, as numerical simulation modeling includes cavitation in both plain and multistep journal bearings. This seeks to ascertain the cavitation region resulting from hydrodynamic lubrication. Figure 14 presents a contour image alongside a graph depicting cavitation distribution.

The highest vapour volume percentage for the simple journal bearing is 0.97, whereas for the multistep journal bearing it is 0.62. The contour indicates that the plain journal bearing possesses a broader cavitation area in comparison to the multistep journal bearing. Figure 15 elucidates the aforementioned statement.

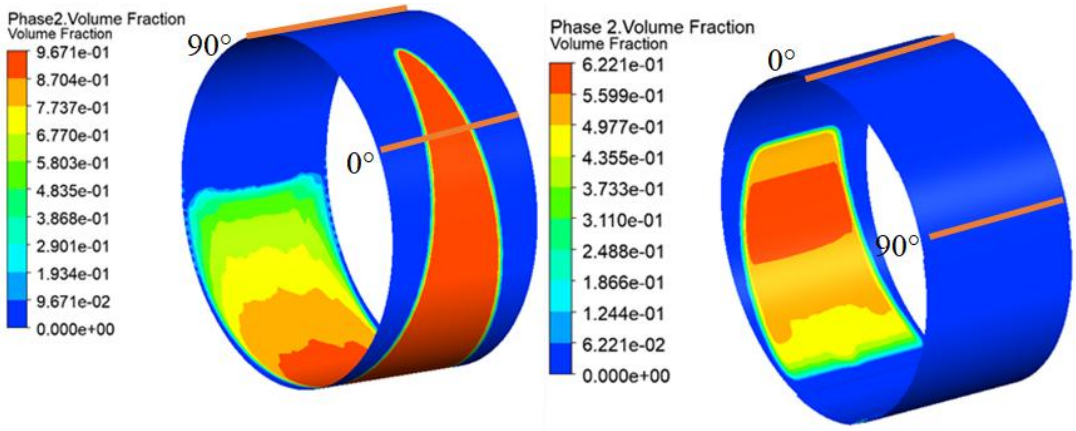

Figure 14: The contour of volume fraction (a) plain journal bearing (b) multistep journal bearing.

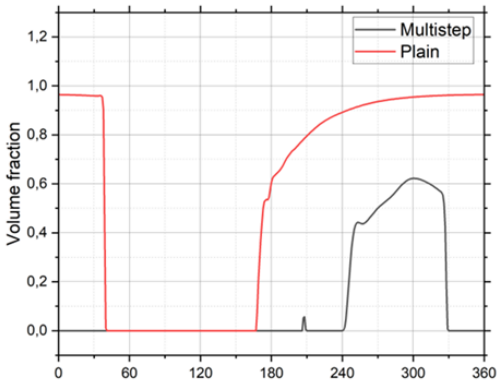

Figure 15: Comparison of the contour volume fraction between both multistep and plain journal bearing.

The contour and cavitation distribution images indicate that the multistep journal bearing exhibits a reduced vapor volume percentage and a constricted cavitation area in comparison to the plain journal bearing. This results from the implementation of a multistep texture, which eliminates cavitation phenomena in each multistep texture. The findings of this study contrast with those of Syafaat et al. (2024), who observed that the implementation of a closed pocket surface texture induced cavitation, but the untextured bearing type did not exhibit cavitation. This discrepancy arises from the distinct construction of the bearings, despite the fact that their performance is fundamentally equivalent. The eccentricity component was absent in Syafaat's analysis due to the parallel bearing configuration between the rotor and stator, which lacks a tilting pad. The inclusion of texture in their research primarily seeks to generate high pressure akin to the eccentricity method utilized in the journal bearing of this study. The eccentricity is the primary determining factor.

It is interesting to note that all the main findings have the potential application to the power-plant and internal combustion engine. We know that in such systems, the lubrication often fails faster than the expected design corresponding to higher load-carrying capacity, and lower friction.

CONCLUSIONS

A study utilizing CFD-FSI has been undertaken on slip and surface roughness in plain and multistep journal bearings. Three surface roughness values were altered in the simulation, and the outcomes were depicted in terms of hydrodynamic pressure, load-carrying capacity, friction force, and structural deformation. The multistep bearing type is often preferable to the plain bearing type. The presence of textured grooves on the surface of multistep bearings enhances oil delivery, hence reducing friction force and increasing load-carrying capacity (LCC) in comparison to plain bearings. Slip engineering influences the LCC and the reduction of frictional force. At minimal surface roughness, the resulting LCC is elevated, whereas an increase in surface roughness leads to a reduction in LCC. High roughness levels might interrupt the flow of the lubricant, resulting in an uneven lubricating film. Furthermore, increased roughness can cause uneven lubricant distribution, resulting in low-pressure zones and lowering the maximum hydrodynamic pressure. Experimental research is the next step in confirming the simulation results.

ACKNOWLEDGEMENTS

This research would not have been possible without full support by RPI (Research Publication International) Grant, No. 973-37/UN7.D2/PP/IX/2024. The authors fully acknowledged Institute for Research and Community Services (LPPM) Diponegoro University for the approved fund, making this important research viable and effective.

REFERENCES

Abd Al-Samieh, M. F. (2019). Surface roughness effects for newtonian and non-newtonian lubricants. Tribology in Industry, 41(1), 56–63.

Adams, T., Grant, C., & Watson, H. (2012). A Simple Algorithm to Relate Measured Surface Roughness to Equivalent Sand-grain Roughness. International Journal of Mechanical Engineering and Mechatronics, 1(1).

ANSYS Inc. (2016). ANSYS FLUENT User's Guide 16.0. Pennsylvania: Canonsburg.

Benasciutti, D., Gallina, M., Munteanu, M. G., & Flumian, F. (2012). A numerical approach for the analysis of deformable journal bearings. Frattura Ed Integrita Strutturale, 21, 37–45.

Bompos, D. A., & Nikolakopoulos, P. G. (2016). Tribological design of a multistep journal bearing. Simulation Modelling Practice and Theory, 68, 18–32.

Bungartz, H. J., & Schäfer, M. (2006). Fluid-structure interaction: Modelling, Simulation, Optimisation. In Lecture Notes in Computational Science and Engineering (Vol. 53).

Chalkiopoulos, M., Charitopoulos, A., Fillon, M., & Papadopoulos, C. I. (2020). Effects of thermal and mechanical deformations on textured thrust bearings optimally designed by a THD calculation method. Tribology International, 148, 106303

Chen, Y., Feng, J., Sun, Y., Peng, X., Dai, Q., & Yu, C. (2020). Effect of groove shape on the hydrodynamic lubrication of journal bearing considering cavitation. Engineering Computations (Swansea, Wales), 37(5), 1557–1576.

Chen, Y., Sun, Y., He, Q., & Feng, J. (2019). Elastohydrodynamic Behavior Analysis of Journal Bearing Using Fluid–Structure Interaction Considering Cavitation. Arabian Journal for Science and Engineering, 44(2), 1305–1320.

Cui, S., Zhang, C., Fillon, M., & Gu, L. (2020). Optimization performance of plain journal bearings with partial wall slip. Tribology International, 145, 106137.

Dhande, D. Y., & Pande, D. W. (2016). Multiphase flow analysis of hydrodynamic journal bearing using CFD coupled Fluid Structure Interaction considering cavitation. Journal of King Saud University - Engineering Sciences, 30(4), 345–354.

Dhande, D. Y., & Pande, D. W. (2017). A two-way FSI analysis of multiphase flow in hydrodynamic journal bearing with cavitation. Journal of the Brazilian Society of Mechanical Sciences and Engineering, 39(9), 3399–3412.

Ebiefung, A. (2019). The Vertical Generalized Complementarity Problem: Mixed Lubrication and Choice of Technology Models. Mathematics and Statistics. 1:45-53.

Galda, L., Sep, J., Olszewski, A., & Zochowski, T. (2019). Experimental investigation into surface texture effect on journal bearings performance. Tribology International, 136, 372–384.

Gropper, D., Wang, L., & Harvey, T. J. (2016). Hydrodynamic lubrication of textured surfaces: A review of modeling techniques and key findings. Tribology international, 94, 509-529.

Gu, C., Meng, X., Wang, S., & Ding, X. (2021). Study on the mutual influence of surface roughness and texture features of rough-textured surfaces on the tribological properties. Proceedings of

the Institution of Mechanical Engineers, Part J: Journal of Engineering Tribology, 235(2), 256–273.
Hili, M. A., Bouaziz, S., Maatar, M., Fakhfakh, T., & Haddar, M. (2010). Hydrodynamic and elastohydrodynamic studies of a cylindrical journal bearing. Journal of hydrodynamics, 22(2),155-163.
Ivanović, L., Vencl, A., Stojanovic, B., & Markovic, B. (2018). Biomimetics design for tribological applications. Tribology in Industry, 40(3), 448–456.
Ji, J. H., Guan, C. W., & Fu, Y. H. (2018). Effect of micro-dimples on hydrodynamic lubrication of textured sinusoidal roughness surfaces. Chinese Journal of Mechanical Engineering (English Edition), 31(4).
Jouini, N., Revel, P., & Thoquenne, G. (2020). Influence of surface integrity on fatigue life of bearing rings finished by precision hard turning and grinding. Journal of Manufacturing Processes, 57(February), 444–451.
Kumar, V., Sharma, S. C., & Narwat, K. (2020). Analysis of control flow valve compensated thrust bearing considering thrust pad flexibility. Jurnal Tribologi, 25(May), 45–58.
Lahmar, M., Ellagoune, S., & Bou-Saïd, B. (2010). Elastohydrodynamic lubrication analysis of a compliant journal bearing considering static and dynamic deformations of the bearing liner. Tribology Transactions, 53(3), 349-368.
Liu, H., Xu, H., Ellison, P. J., & Jin, Z. (2010). Application of computational fluid dynamics and fluidstructure interaction method to the lubrication study of a rotor-bearing system. Tribology Letters, 38(3), 325–336.
Lu, X., & Khonsari, M. M. (2007). An experimental investigation of dimple effect on the stribeck curve of journal bearings. Tribology Letters, 27(2), 169–176.
Meng, F., Wei, Z., Minggang, D., & Gao, G. (2016). Study of acoustic performance of textured journal bearing. Proceedings of the Institution of Mechanical Engineers, Part J: Journal of Engineering Tribology, 230(2), 156–169.
Muchammad M., Tauviqirrahman M., Farhansyah S., Iqbal M., Setiyana B., Jamari J. (2024). Elastohydrodynamic analysis of composite material with roughness effect on multistep journal bearing tribological performance. Jurnal Tribologi, 40, 39-60.
Muchammad, M., Tauviqirrahman, M., Jamari, J., & Schipper, D. J. (2020). Analysis of the effect of the slip-pocket in single and double parallel bearing considering cavitation: A theoretical approach. Lubricants, 9(1), 3.
Muchammad, M., Tauviqirrahman, M., Soetopo, H.S.S., & Jamari, J. (2021) Mechanical and thermal deformations effects on plain journal bearing with isoviscous boundary condition based on CFD and FSI methods. Jurnal Tribologi, 28, 63-81.
Oliveira, M. V. M., Fioravanti, A. R., & Daniel, G. B. (2022). Identification of oil starvation in hydrodynamic journal bearing using rotor vibration and Extended Kalman Filter. Tribology International, 169.
Prabhakaran Nair, K., Sukumaran Nair, V. P., & Jayadas, N. H. (2007). Static and dynamic analysis of elastohydrodynamic elliptical journal bearing with micropolar lubricant. Tribology International, 40(2 SPEC. ISS.), 297–305.
Sander, D. E., Allmaier, H., Priebsch, H. H., Witt, M., & Skiadas, A. (2016). Simulation of journal bearing friction in severe mixed lubrication: Validation and effect of surface smoothing due to running-in. Tribology international, 96, 173-183.
Sayed, H., & El-Sayed, T. A. (2022). A novel method to evaluate the journal bearing forces with application to flexible rotor model. Tribology International, 173.

Shenoy, B. S., Pai, R. S., Rao, D. S., & Pai, R. (2010). Elasto-hydrodynamic lubrication analysis of full 360° journal bearing using CFD and FSI techniques. World Journal of Modelling and Simulation, 6(4), 315–320.

Shi, X., & Ni, T. (2011). Effects of groove textures on fully lubricated sliding with cavitation. Tribology International, 44(12), 2022–2028.

Syafaat, I., Nugroho, A., Sodikin, M., Hida, A. A., Ratnani, R. D., Setiyana, B., Muchammad, M., & Tauviqirrahman, M. (2024). A 3D design of the hydrodynamic pocketed thrust bearing with slip engineered for eliminating cavitation. Results in Engineering, 24, 103039.

Tauviqirrahman, M., Afif, M. F., Pujiyanto, M., Surojo, E., Setiyana, B., & Jamari, J. (2020). Numerical simulation of journal bearing considering cavitation and thermal effect. Proceedings of the 3rd International Conference on Engineering and Applied Technology, 2320, 020035.

Tauviqirrahman, M., Ichsan, B. C., Jamari, & Muchammad. (2019). Influence of roughness on the behavior of three-dimensional journal bearing based on fluid-structure interaction approach. Journal of Mechanical Science and Technology, 33(10), 4783–4790.

Tauviqirrahman, M., Muthik, B., Muchammad, M., Pratomo, A. W., & Jamari, J. (2016). Effect of cavitation modelling on the prediction of the lubrication performance using CFD: A case study of journal bearing lubricated with non-newtonian. International Journal of Engineering and Technology, 8(6), 2541–2546.

Tønder, K. (2001). Inlet roughness tribodevices: dynamic coefficients and leakage. Tribology International, 34(12), 847-852.

Wang, W., Zhou, D., Shen, L., Zhang, J., & Wang, X. (2018). Effects of elastic deformation on hydrodynamic lubrication of heterogeneous textured journal bearing. Proceedings of the Institution of Mechanical Engineers, Part J: Journal of Engineering Tribology, 232(3), 292–309.

Xiao, Y. F., Liu, J., & Yang, S. P. (2020). Thermal coupled elastohydrodynamic lubrication analysis of journal bearing considering thermal effect and cavitation. Proceedings of the Institution of Mechanical Engineers, Part J: Journal of Engineering Tribology, 234(6), 939–953.

Zhu, Z. W., Xia, W. X., & Zhang, Y. X. (2017). Effects of surface topography on journal bearing lubrication considering cavitation. Tribology International, 115, 451–461.